

SUBMITTED TO "MECHANICS OF MATERIALS" ON 4th OCTOBER 2020

**Rate-dependent adhesion of viscoelastic contacts. Part I: contact area and contact line velocity within model multi-asperity contacts with rubber.**

G. Violano,<sup>1</sup> A. Chateauminois,<sup>2</sup> and L. Afferrante<sup>1,\*</sup>

<sup>1</sup>*Department of Mechanics, Mathematics and Management,  
Polytechnic University of Bari, Via E. Orabona, 4, 70125, Bari, Italy*

<sup>2</sup>*Soft Matter Science and Engineering Laboratory (SIMM),  
PSL Research University, UPMC Univ Paris 06,  
Sorbonne Universités, ESPCI Paris, CNRS,  
10 rue Vauquelin, 75231 Paris cedex 05, France*

arXiv:2012.07779v1 [cond-mat.soft] 14 Dec 2020

## Abstract

In this work, we investigate dissipative effects involved during the detachment of a smooth spherical glass probe from a viscoelastic silicone substrate patterned with micro-asperities. As a baseline, the pull-off of a single asperity, millimeter-sized contact between a glass lens and a smooth poly(dimethylsiloxane) (PDMS) rubber is first investigated as a function of the imposed detachment velocity. From a measurement of the contact radius  $a(t)$  and normal load during unloading, the dependence of the strain energy release rate  $G$  on the velocity of the contact line  $v_c = da/dt$  is determined under the assumption that viscoelastic dissipation is localized at the edge of the contact. These data are incorporated into Muller's model (V.M. Muller *J Adh Sci Tech* (1999) **13** 999-1016) in order to predict the time-dependence of the contact size. Similar pull-off experiments are carried out with the same PDMS substrate patterned with spherical micro-asperities with a prescribed height distribution. From *in situ* optical measurements of the micro-contacts, scaling laws are identified for the contact radius  $a$  and the contact line velocity  $v_c$ . On the basis of the observed similarity between macro and microscale contacts, a numerical solution is developed to predict the reduction of the contact radius during unloading.

Keywords: viscoelasticity, adhesion, surface roughness, energy release rate.

---

\*Electronic address: [guido.violano@poliba.it](mailto:guido.violano@poliba.it)

## I. INTRODUCTION

Adhesion is of paramount importance in the contact mechanics of micro and nano systems [1] as, at the molecular scale, adhesive interactions between atoms are ‘strong’ compared to the usual forces acting between bodies [2]. However, adhesion is seldom observed at the macroscopic scale due to surface roughness, which reduces the area of real contact. Nevertheless, when dealing with very soft matter, strong adhesion may be still detected even in presence of surface roughness [3].

Soft matter adhesion finds applications in several fields, e.g. design of pressure-sensitive-adhesives (PSA) [4], soft robots [5] and new technologies inspired by biotribological systems [6].

In most of adhesion tests on soft compliant spheres [3, 7], the measured detachment force is generally greatly in excess of that predicted by Johnson, Kendall & Roberts (JKR) theory [8] and the detachment process is observed to be dependent on the rate of separation [9].

The JKR theory applies for purely elastic spheres and under quasi-static conditions. In experimental investigations, the pull-off process unlikely obeys the quasi-static conditions and the effective work of adhesion  $\Delta\gamma_{\text{eff}}$  depends on the velocity  $v_c$  of the contact line during pull-off. Namely,  $\Delta\gamma_{\text{eff}}$  may be strongly increased with respect to the quasi-static value  $\Delta\gamma_0$  as a result of viscous dissipation, where  $\Delta\gamma_0$  follows the well-known Dupré’s equation  $\Delta\gamma_0 = \gamma_1 + \gamma_2 - \gamma_{12}$ , being  $\gamma_1$ ,  $\gamma_2$  the adhesive energies of the two contacting surfaces and  $\gamma_{12}$  the interaction term.

Gent & Schultz (GS) [10] observed that viscous effects are exclusively located close to the crack tip. Maugis & Barquins (MB) [11] proposed a generalization of the JKR theory, showing that the dependence of  $\Delta\gamma_{\text{eff}}$  on  $v_c$  can be expressed in terms of a dissipation function  $f(v_c, T)$  related to the viscoelastic properties of the material and depending on the crack tip velocity  $v_c$  and the temperature  $T$ . In particular, MB showed that, for a given elastomer, the effective work of adhesion  $\Delta\gamma_{\text{eff}}$  is a universal function of the crack tip velocity  $v_c$ . Moreover, performing experimental tests on three different geometries (spheres, punches and tapes (peeling)), MB found that the dependence of  $\Delta\gamma_{\text{eff}}$  on  $v_c$  is not affected by the geometry and loading system. In MB’s solution, viscous effects are assumed not involving bulk deformations as “*gross displacements must be elastic for  $G$  to be valid in kinetic phenomena*”, being  $G$  the energy release rate, i.e. the amount of energy required to

advance a fracture plane by a unit area. Robbe-Valloire & Barquins [12] extended MB studies performing adherence experiments between a rigid cylinder and an elastomeric solid. They confirmed the existence of a master curve for  $f(v_c, T)$ . Specifically, their results ”*prove once again that the master curve drawn and its variation... is a characteristic of the propagation in mode I at the interface of our rubber-like material, when viscoelastic losses are closely limited to the crack tip, so that  $G$  can be calculated from the theory of linear elasticity.*”

More recently, Muller [13] showed that the process of detachment of viscoelastic spheres can be described by a first-order differential equation, whose solution is based on the assumption originally proposed in Ref. [10]. Alternative approaches taking into account bulk deformations were proposed by the group of Barthel in Refs. [14–16].

In this work, we present an experimental investigation of dissipative effects involved in the adhesion between a rough contact interface between a smooth spherical glass probe and a viscoelastic silicone substrate patterned with a prescribed height distribution of micrometer sized spherical asperities. Taking advantage from the fact that the size of these micro-asperities (radius of 100  $\mu\text{m}$ ) allows for an optical measurement of the space distribution of micro-contact areas, such patterned surfaces obtained from micro-milling techniques were previously successfully used to probe the elastic interactions between micro-asperity contacts [17] or to investigate adhesive equilibrium of rough contact interfaces [18]. Here, we focus on the effects of viscoelastic dissipation on the rate-dependence of micro-contact sizes during unloading at a imposed velocity using JKR-type experiments. The investigation of adhesive behaviour at the level of micro-contact spots is inspired by the Roberts’ statement (Ref. [19]): ”*The contact of a smooth centimeter-sized rubber sphere may be regarded as that of a giant single asperity...The ability to predict the adhesion forces on a large asperity is a step towards building up a model of a real surface of micron-sized asperities, which approximate to an array of minute hemispheres of different height and radius*”.

Accordingly, pull-off experiments have first been conducted on smooth PDMS surfaces to investigate the adhesion behavior at the macroscopic scale. Specifically, under the assumption of viscous effects located only near the detachment front, we propose a very simple methodology to calculate the time-dependent radius of the contacts during unloading by exploiting the Muller’s approach [13] which was already used to calculate the adhesion hysteresis occurring in loading-unloading tests performed on smooth viscoelastic spheres [20]. Then, this approach is successfully extended at the micro-scale with no need to incorporate

a size-dependence in the relationship ruling the dependence of the strain energy release rate on the velocity of the contact line.

## II. DETACHMENT OF VISCOELASTIC SPHERES

In order to detach a soft body from a rigid substrate, the force required to create a new unit length of crack is  $(G - \Delta\gamma_0)$ . If the energy release rate  $G$  is larger than the adiabatic work of adhesion  $\Delta\gamma_0$ , the crack opens and the detachment process advances.

Gent & Schultz (GS) [10] found that

$$G - \Delta\gamma_0 = \Delta\gamma_0 \cdot f(v_c, T) \quad (1)$$

where  $\Delta\gamma_0 \cdot f(v_c, T)$  is the drag due to viscoelastic losses at the crack tip, being  $v_c = -da/dt$  the velocity of the contact line. The above relation usually works for  $v_c$  ranging from  $10^{-5}$  cm/s to 1 cm/s [19, 21–23] and allows to predict the kinetics of detachment (see Maugis & Barquins [11]).

The function  $f(v_c, T)$ , which is found to be independent of the geometry and loading system, can be described by the phenomenological equation

$$f(v_c) = k(a_T v_c)^n, \quad (2)$$

where  $k$  and  $n$  are characteristic constants of the material and  $a_T$  is the William-Landel-Ferry (WLF) factor [24] accounting for the dependence of  $f(v_c, T)$  on the temperature  $T$ . Eq. (2) also accounts for the dependence of  $G$  on the relaxed elastic modulus  $E$  (Ref. [25]), whose frequency dependence appears only at the crack tip [26].

Introducing eq. (2) in (1), we obtain

$$G = \Delta\gamma_0[1 + c \cdot v_c^n], \quad (3)$$

with  $c = k \cdot a_T^n$ .

For a given elastomer, the values of  $c$  and  $n$  can be obtained by fitting the experimental data relating  $G$  and  $v_c$ . As observed in Ref. [7], the exponent  $n$  *”is not a universal number, but takes different values depending on viscoelastic modulus”*.

### A. Muller's model

Muller [13] proposed a two-parameters differential equation to describe the detachment of a viscoelastic sphere of radius  $R$  and Young modulus  $E^*$  from a rigid substrate

$$\frac{d\bar{a}}{d\bar{\delta}} = \left[ \frac{\Delta\gamma_0}{RE^*} \right]^{1/3} \cdot \frac{1}{\beta} \left[ \bar{a}^3 \left( 1 - \frac{\bar{\delta}}{3\bar{a}^2} \right)^2 - \frac{4}{9} \right]^{1/n}, \quad (4)$$

where  $\bar{a} = a / \left[ 3R(\pi\Delta\gamma_0/(6E^*R))^{1/3} \right]$  and  $\bar{\delta} = \delta / \left[ 3R(\pi\Delta\gamma_0/(6E^*R))^{2/3} \right]$  are the dimensionless contact radius and penetration, respectively, and the parameter  $\beta$  is proportional to the driving velocity  $V$

$$\beta = \left( \frac{6}{\pi} \right)^{1/3} \left( \frac{4}{9}c \right)^{1/n} V. \quad (5)$$

Muller's model moves from two assumptions: i) viscous effects are located exclusively near the crack tip; ii) detachment occurs under constant  $V$ . The energy release rate  $G$ , which represents the effective work of adhesion  $\Delta\gamma_{\text{eff}}$  required to break the contact, can be evaluated as

$$G = \frac{(F_H - F)^2}{6\pi RF_H} \quad (6)$$

where  $F_H = 4/3E^*a^3/R$  is the Hertzian load and  $F$  is the applied load. Eq. 6 is only valid under the assumption of viscous effects concentrated at the crack tip (see, for example, Ref. [32]).

### III. EXPERIMENTAL SET-UP

JKR-like tests were carried out between an optical spherical glass lens and rubber substrates. The glass indenter, which is assumed to be smooth, has a radius of curvature  $R_{\text{sphere}}$  of 103.7 mm. Rubber substrates are made of commercially available PolyDiMethyl-Siloxane (PDMS) silicones. Samples were manufactured by cross-linking at 70 °C for 48 hours a mixture of Sylgard 184 and Sylgard 527 silicones (Dow Chemicals), with a 0.35:0.65 weight ratio. As detailed by Palchesko et al. [27], mixing these two silicone elastomers in different ratios allows to tune the elastic modulus in between a few kPa and 3 MPa. As compared to raw Sylgard 184, the Young's modulus of the selected Sylgard 184:Sylgard 527 mixture ( $E = 0.83$  MPa, see below) was decreased by a factor of about 3.6, with the aim

of enhancing the adhesion properties. In addition, crosslinking simultaneously these two different silicone products was expected to result in an increased concentration of network defects such as dangling chains. As detailed in Ref. [27], such imperfections are known to enhance the viscoelastic dissipation of silicone networks.

Fig. 1 shows a sketch of the experimental set-up. The spherical indenter is fixed to a motorized vertical translation stage by means of a double cantilever beam of known stiffness ( $290 \text{ N m}^{-1}$ ). The value of the applied load is obtained from the deflection of the cantilever, as it is measured using a high resolution optical sensor (Philtec D64-L). Due to the compliance of the double cantilever beam, the actual velocity of the lens can slightly differ from the prescribed velocity. In order to account for this effect, a laser displacement sensor (Keyence LK-H057) is used to monitor the actual position of the lens. The difference between the prescribed and actual velocity of the indenter were found to be significant only for the macroscopic single asperity contact close to pull-off, when the greatest tensile normal forces are achieved.

The PDMS sample is fixed to two crossed motorized linear translation stages, which allow to change the relative position of the rubber sample with respect to the indenter. A LED light spot is installed to illuminate in transmission the contact area. Once illuminated, contact pictures are recorded through the transparent PDMS using a zoom objective (Leica APO Z16) and a high resolution CMOS camera (SVS Vistek Exo,  $2048 \times 2048$  pixels<sup>2</sup>, 8 bits).

### 1. *Experiments on smooth samples*

The contact radius vs. load data obtained by indentation experiments on smooth PDMS samples were fitted according to the JKR theory [8] in order to evaluate the reduced elastic modulus ( $E^* = 0.83 \text{ MPa}$ ) and the adhesion energy ( $\Delta\gamma_0 = 0.037 \text{ J/m}^2$ ). During loading, contact tests have been performed under fixed load conditions. Specifically, the applied load is increased step by step and, once each load step is reached, contact is maintained for a long time (800 s) to ensure that adhesive equilibrium is reached (with viscoelastic effects totally relaxed [18]).

Unloading tests are performed at imposed driving velocity of the vertical stage, while continuously monitoring the lens position, the applied force and the contact radius. Experi-

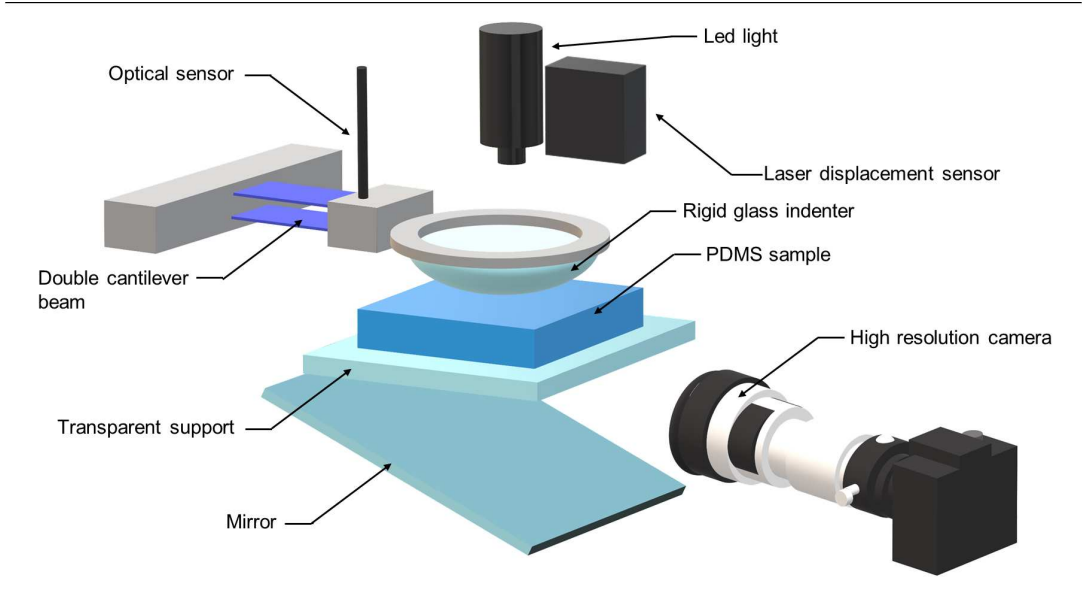


FIG. 1: The experimental setup of JKR adhesion tests.

ments are performed at three different values of the driving velocity  $V = 0.02, 0.002, 0.0002$  mm/s. Three contact realizations have been carried out for each velocity.

## 2. Experiments on rough samples

PDMS samples were textured with a statistical distribution of spherical micro-asperities with the same radius of curvature. The patterned surface was obtained by moulding PDMS in PolyMethylMethAcrylate (PMMA) forms milled using ball-end mills with a radius of  $100 \mu\text{m}$ . In order to enhance adhesive effects, a smoothing of the spherical cavities of the PMMA molds has been achieved by exposing them to a saturated  $\text{CHCl}_3$  vapor for 30 minutes. As detailed in Ref. [18], such treatment leads to a slight increase in the radius of the spherical bumps, up to a 10% enhancement.

The patterned surface has been generated with a squared nominal area of  $10 \text{ mm}^2$ , where asperities are randomly distributed with a density of  $2 \times 10^7 \text{ m}^{-2}$ . The spherical caps present heights distributed according to a Gaussian law with standard deviations  $\sigma = 5 \mu\text{m}$ .

Asperities are collocated with a non-overlapping constraint. For the considered surface density, each contacting asperity behaves as an isolated spherical punch and lateral interactions can be neglected as shown in Refs. [17, 18]. We stress that such assumption is no longer valid when roughness on several length scales is considered like in the case of



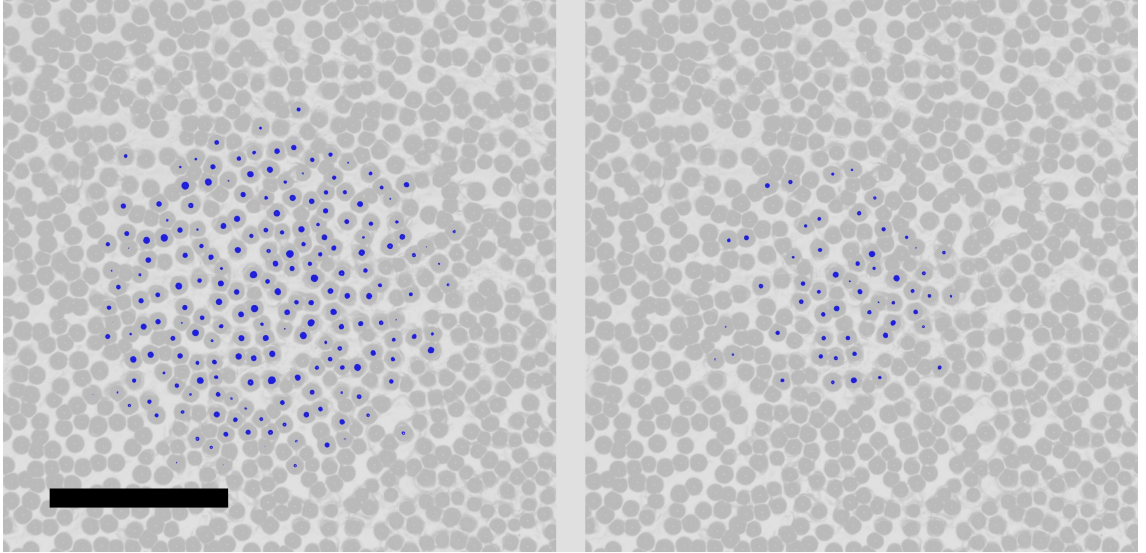


FIG. 2: Detachment of spherical micro-asperities. The contact spots (blue disks) are detected after post-processing of the contact pictures. The length of the black rectangle is 1 mm.

self-affine fractal geometries [28–30].

Fig. 2 shows images of contact micro-spots (blue disks) during unloading. Accurate measurements of the area of contact spots is achieved by image processing after background removal. During unloading, experiments have been performed at the same values of driving velocity  $V$  used in the tests conducted on smooth samples ( $V = 0.02, 0.002, 0.0002$  mm/s).

## IV. RESULTS

### A. Smooth contact: macroscopic scale

Fig. 3 shows the contact radius  $a$  as a function of the applied load  $F$ , during unloading. Results are obtained for different values of the driving velocity  $V$ . Three contact tests were performed for each  $V$  and the average values are reported in the plot.

The detachment process is clearly rate-dependent as great adhesion enhancement is observed by increasing  $V$ , as indicated by the increase in pull-off force.

Fig. 4A shows, in a semilogarithmic representation, the reduction of the contact radius

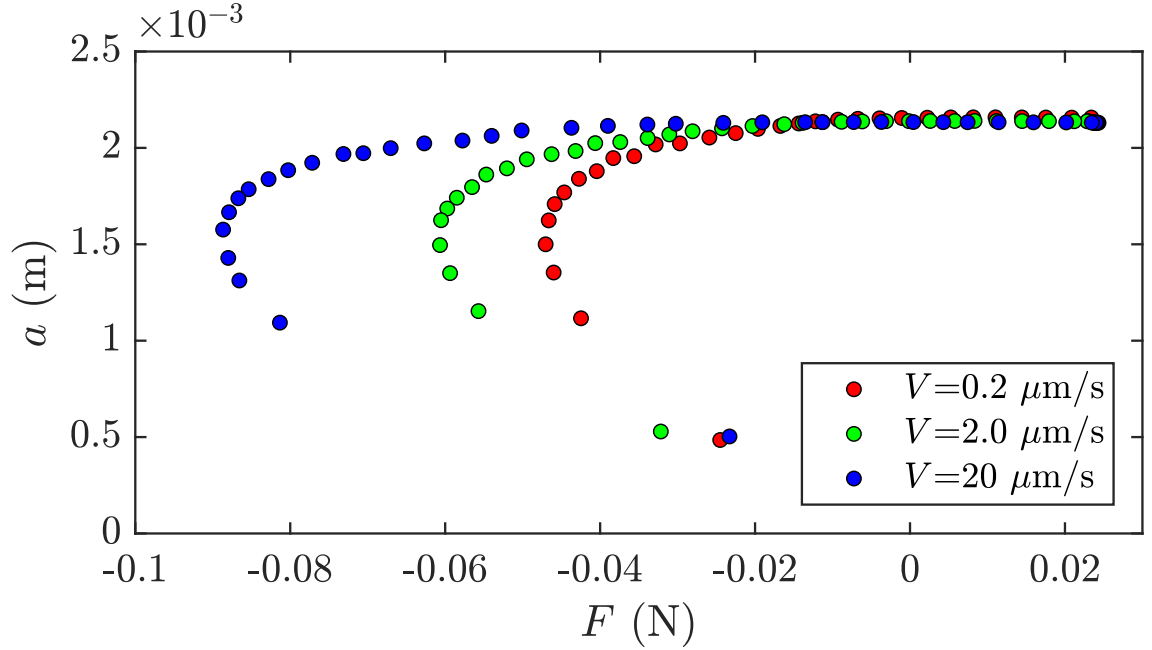


FIG. 3: The contact radius  $a$  as a function of the applied load  $F$ . Results are shown for different unloading velocities of the indenter  $V = 0.02, 0.002, 0.0002$  mm/s. For each velocity three tests have been performed and the average values are reported in the plot.

$a$  with the time  $t$ . Experimental data are fitted according to the following relation

$$a(t) = p_1 \sqrt{\left(1 - \frac{t}{t_{po} + 1}\right)^{p_2}} \quad (7)$$

where  $t_{po}$  is the instant at which detachment occurs and  $p_1, p_2$  are fitting parameters.

During detachment, the crack tip velocity can be easily obtained as  $v_c = -da/dt$ . Fig. 4B shows the curves  $a$  vs.  $v_c$  obtained in the experiments at different velocities. The maximum value of  $v_c$  is reached when abrupt pull-off occurs. Notice that when increasing  $V$  of one order of magnitude the same enhancement in  $v_c$  is also observed.

The effective work of adhesion  $G$  is calculated as a function of measured contact line velocity by eq. (6) using the experimental value of the normal load  $F$ . As discussed by Barquins [31], the resulting  $G(v_c)$  relationship is unaffected by the machine compliance. The actual stiffness of the system is taken into account because the load  $F$  is read from the deflection of the double cantilever beam. The same procedure has been recently used in Ref. [32], where the effective work of adhesion is measured in spherical contact between a glass lens and PDMS blocks.

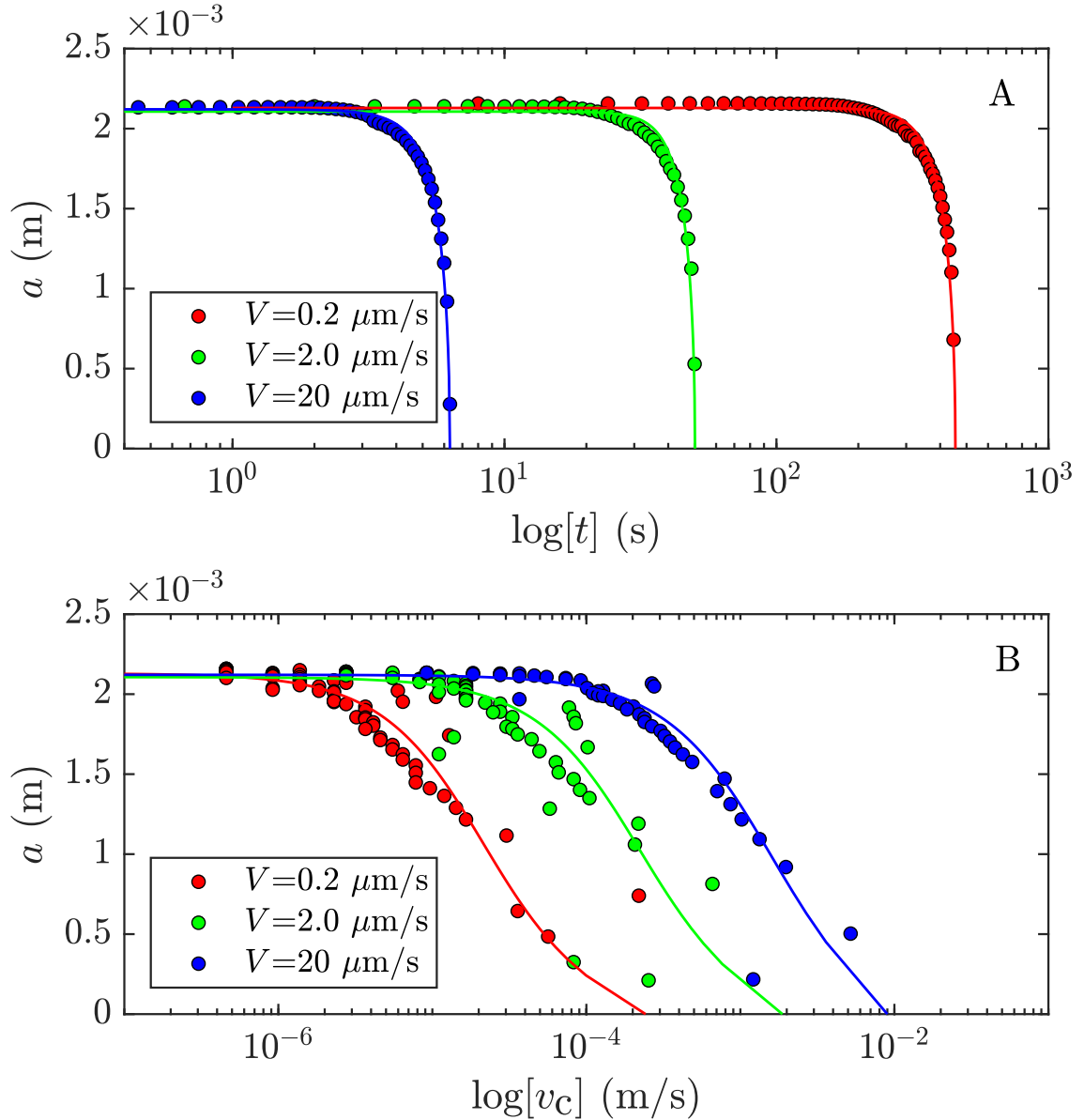


FIG. 4: A: The contact radius  $a$  as a function of the time  $t$ . Results show the average of three contact tests. Blue, green and red markers are referred to the unloading velocities of the indenter  $V = 0.02, 0.002, 0.0002$  mm/s, respectively. Solid lines denote the fit of experimental data. B: The contact radius  $a$  as a function of the crack tip velocity  $v_c$ . Legend symbols are the same of A.

Fig. 5 shows the quantity  $(G - \Delta\gamma_0)/\Delta\gamma_0$  as a function of  $v_c$  in a double logarithmic representation. Markers denote experimental data, while the dotted black line is the fit obtained with eq. (3) using  $c = 31$  and  $n = 0.25$ . Maugis & Barquins [11] found  $n = 0.6$  for a viscoelastic polyurethane rubber. More recently, Lorenz et al. [7] found  $n = 0.19$  for polyurethane and  $n = 0.12$  for Sylgard 184 PDMS rubber. As discussed by Barthel

and Frétiigny [16], the dependence of  $G$  on the crack tip velocity can be related to the viscoelastic creep function of the solids. Accordingly, the fact that we found for the used Sylgard 184:Sylgard 527 mixture an exponent  $n$  greater than for raw Sylgard 184 probably reflects the enhanced viscoelastic dissipation of the PDMS mixture.

The values of  $c$  and  $n$  can be used in eq. (5) to calculate the values of  $\beta$  required in Muller's model. According to Muller's model, eq. (4) can be numerically integrated to obtain  $a(\delta)$ . Assuming that  $V$  is constant during unloading, the instant  $t_{\text{po}}$  at which pull-off occurs can be estimated by  $t_{\text{po}} = (\delta_0 - \delta_{\text{po}})/V$ , where  $\delta_0$  is the initial penetration and  $\delta_{\text{po}}$  the jump-off distance. However, in our experiments we found that the actual unloading velocity  $V_{\text{act}}(t)$  is not constant as the spherical indenter is held to the stage using a compliant double cantilever beam. Due to the deflection of the beam, the velocity  $V_{\text{act}}$  of the lens can be different from the imposed velocity  $V$ . This is especially true for the experiments on smooth PDMS, where high forces can be achieved. However this effect is quantified by the laser displacement sensor, which monitors the actual position  $z(t)$  of the lens. Hence, the actual velocity is derived as  $V_{\text{act}}(t) = \Delta z / \Delta t$ . In the original Muller's model, the unloading velocity  $V = -d\delta/dt$  is assumed to be constant. However, we can modify eq. (5) by introducing the actual velocity  $V_{\text{act}}(\delta)$  in the parameter  $\beta$

$$\beta = \left(\frac{6}{\pi}\right)^{1/3} \left(\frac{4}{9}c\right)^{1/n} V_{\text{act}}(\bar{\delta}). \quad (8)$$

where  $V_{\text{act}}(\delta)$  is obtained by interpolating experimental data.

The time required to move from  $\delta_0$  to a generic  $\delta$  is then calculated as

$$t = \int_{\delta_0}^{\delta} \frac{\delta}{V_{\text{act}}(\delta)} d\delta. \quad (9)$$

Results are shown in Figs. 6A-C, where the contact radius  $a(t)$ , normalized with respect to its initial value, is plotted against the time normalized with respect to the period required for pull-off to occur. Results are given for different unloading velocities and show a good agreement between experimental data and numerical predictions.

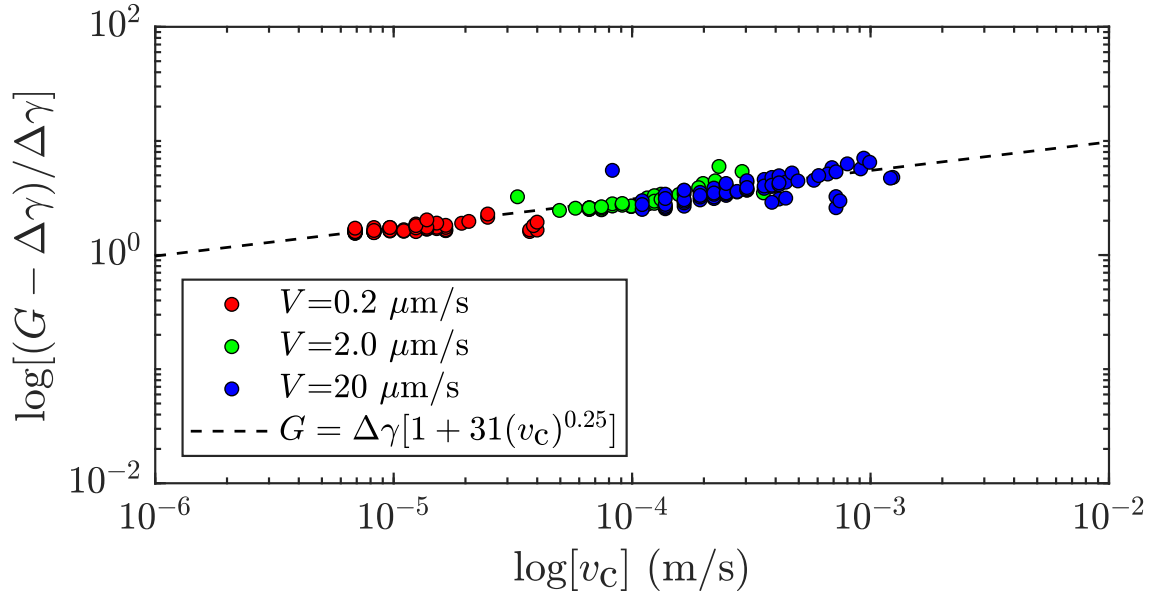


FIG. 5: The relative increase  $(G - \Delta\gamma_0)/\Delta\gamma_0$  as a function of the crack tip velocity  $v_c$ . Results are shown for three contact realizations. Blue, green and red markers are referred to the unloading velocities of the indenter  $V = 0.02, 0.002, 0.0002 \text{ mm/s}$ . The dotted line is the fit obtained with eq. (3).

### B. Rough contact: microscopic scale

In the experiments performed on rough samples the number of micro-asperities detected in contact at the end of the loading phase is around 160. However, for the sake of clarity, Figs. 7A and 7B show the variation of the contact radius  $a$  of 8 micro-asperities in terms of the time and the contact line velocity  $v_c$ , respectively. Results are shown for  $V = 2 \times 10^{-4} \text{ mm/s}$ . In general, asperities with a larger value of the initial contact radius  $a$  require a longer time to complete their detachment process.

Results on smooth and rough samples suggest the existence of scale effects on both contact radius  $a$  and detachment front velocity  $v_c$ . For this reason, we rescale the above results introducing the factors  $s_a = a_{0\text{macro}}/a_{0i}$ ,  $s_t = t_{\text{po-macro}}/t_{\text{po-i}}$  and  $s_v = s_a/s_t$ . The quantity  $a_{0\text{macro}}$  is the initial value of the contact radius measured at the macroscale on smooth PDMS samples at the end of the loading phase (when unloading starts);  $a_{0i}$  is instead the initial value of the contact radius detected for the  $i^{\text{th}}$  micro-asperity. Similarly,  $t_{\text{po-macro}}$  is the time at which pull-off occurs at the macroscale (that is measured in the tests performed on smooth PDMS samples), while  $t_{\text{po-i}}$  is the time required (and measured in the tests on rough PDMS samples) to detach the  $i^{\text{th}}$  micro-asperity.

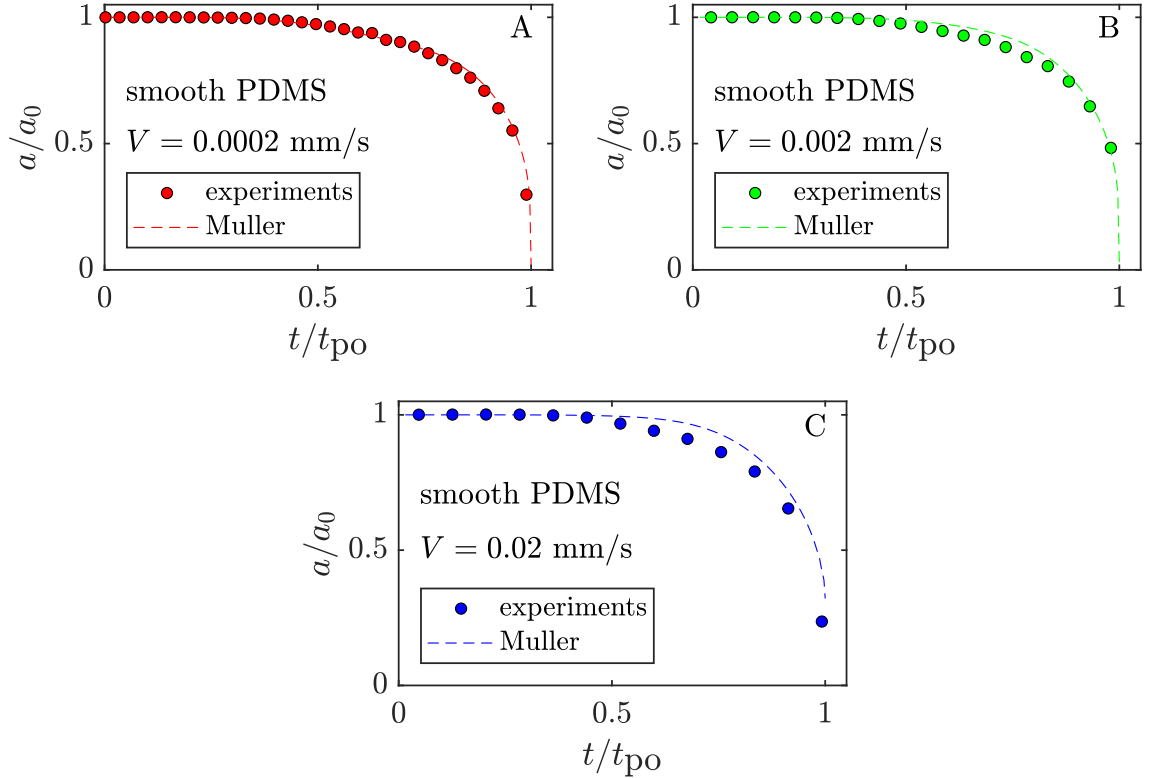


FIG. 6: A-C: The time dependence of the normalized contact radius  $a(t)$ . Results are shown for unloading velocity of the indenter  $V = 0.0002, 0.002, 0.02$  mm/s (figs. A,B,C respectively). Dashed lines denote Muller’s model predictions, while markers experimental data, which are averaged on three contact realizations.

Therefore, contact radius  $a$ , crack tip velocity  $v_c$  and time are rescaled with the above factors. The new curves are given in Fig. 8 for three different driving velocities  $V$  and in a semi-log plot. Solid lines denote the curves obtained at the macroscopic scale in the experiments conducted on smooth substrate. Dashed lines identify the curves measured for each micro-asperity during the detachment tests performed on the rough PDMS samples. All curves obtained on the contact microspots almost collapse on the curves measured at the macroscale (smooth samples). Such result suggests that the distributions of the actual crack-tip velocities  $v_c$ , which are achieved locally at micro-contact, scale during contact unloading. This, in turn, suggests that the parameters of Muller’s model identified at the macroscale can be applied to the microcontacts.

Such an assumption finds also its motivation in recent results by Lorentz et al. [7], who performed adhesion experiments on smooth spheres of different radii (ranging from  $R \approx 3$  mm to  $R = 46.5$  mm) and different materials. They deduced  $\Delta\gamma_{\text{eff}}$  as a function of the

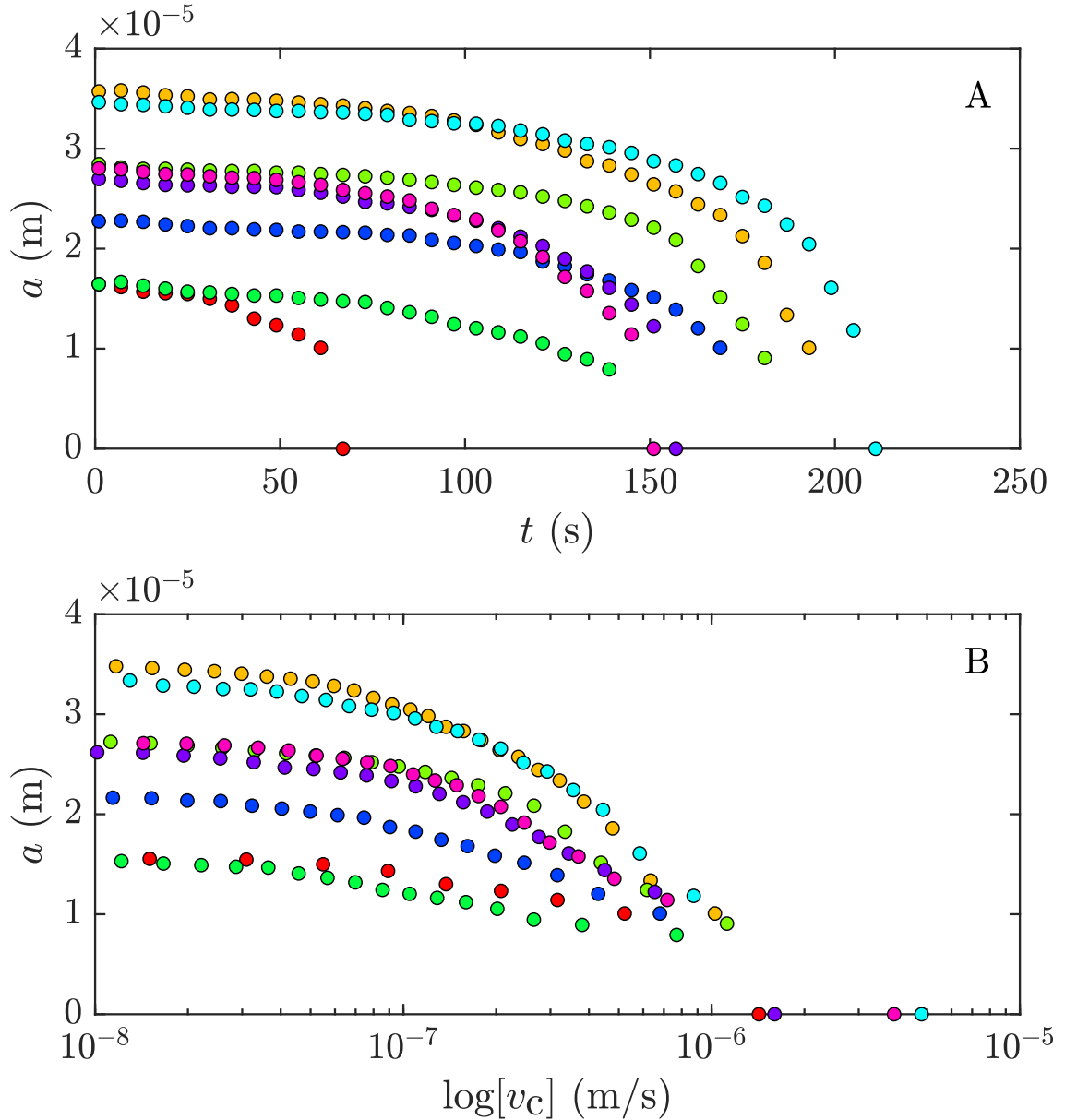


FIG. 7: A: The contact radius  $a$  of micro-asperities as a function of time  $t$ . Markers denote experimental data for a selection of eight different micro-contacts. Unloading tests are performed at  $V = 0.0002$  mm/s. B: The contact radius  $a$  as a function of the crack tip velocity  $v_c$ .

contact line velocity  $v_c$  using the JKR theory and observed that the experimental data exhibited the same velocity dependence as calculated by eq. (1) for  $v_c < 10^{-4}$  m/s (which corresponds to the range of crack tip velocities measured in our experiments on micro-spots).

The same plots given in Figs. 6 are reported in Figs. 9 for each of the micro-contacts detected during the unloading phase. A satisfactory good agreement is found between

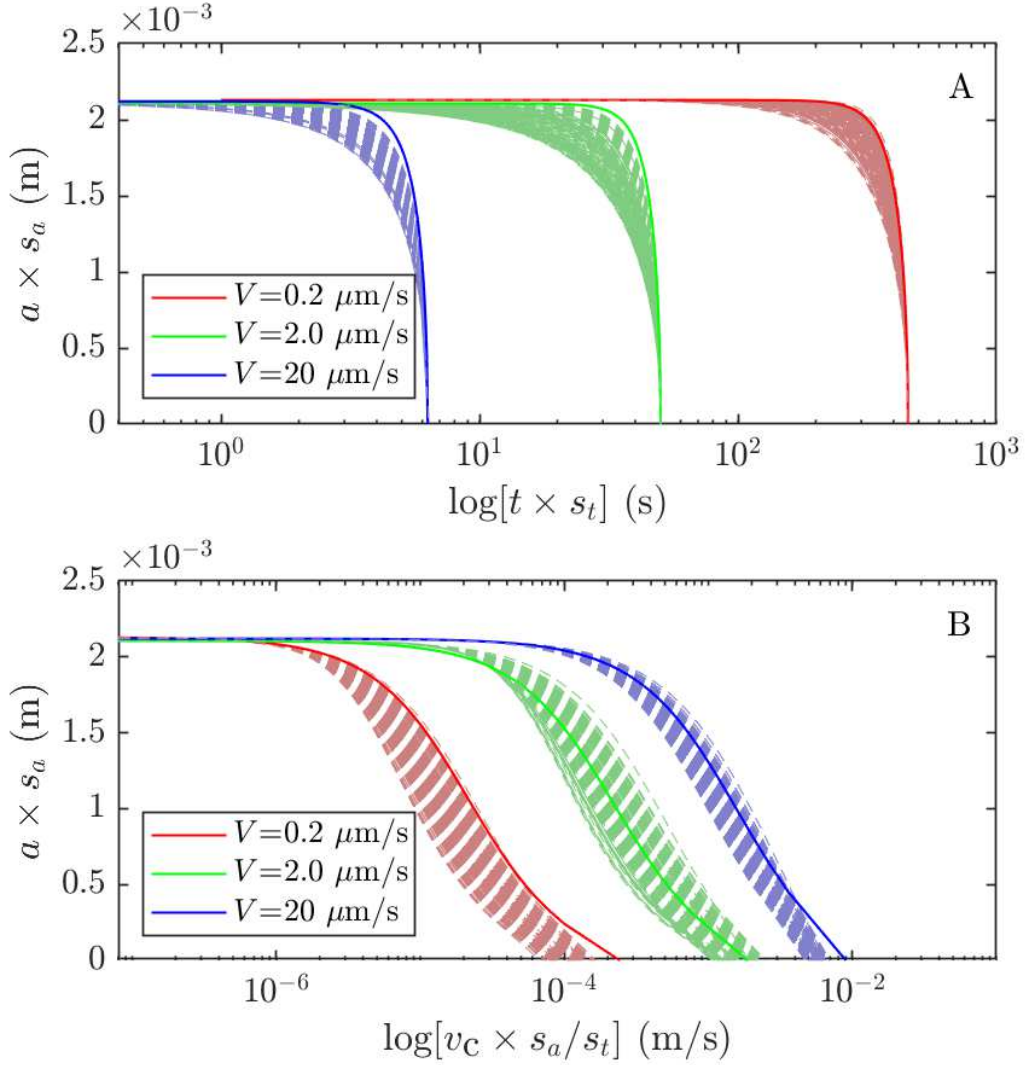


FIG. 8: A: The contact radius  $a \times s_a$  as a function of time  $t \times s_t$  (semilog scale). Solid lines denote the smooth macro-spot detachment curve. Dashed lines denote the detachment curves of 160 micro-asperities. Red, Green and Blue curves refer to  $V = 0.2, 2.0, 20, \mu\text{m/s}$ . A: B: The contact radius  $a \times s_a$  as a function of the crack tip velocities  $v_c \times s_a/s_t$  (semilog scale). Legend symbols are the same of A.

experimental data and numerical predictions, which are obtained with the "macroscale" values of  $c$  and  $n$ . Also in this case, in the Muller's model, we have introduced the actual value of the unloading velocity, which is however constant and slightly lower than the imposed one ( $V_{\text{act}} = 0.8V$ ). In the  $a - t$  curves, we can distinguish a period of time where stick adhesion is observed with an almost constant contact radius (i.e. the contact line velocity is zero). This "stick time" is negligibly influenced by the initial value  $a_0$  of the contact radius [15].



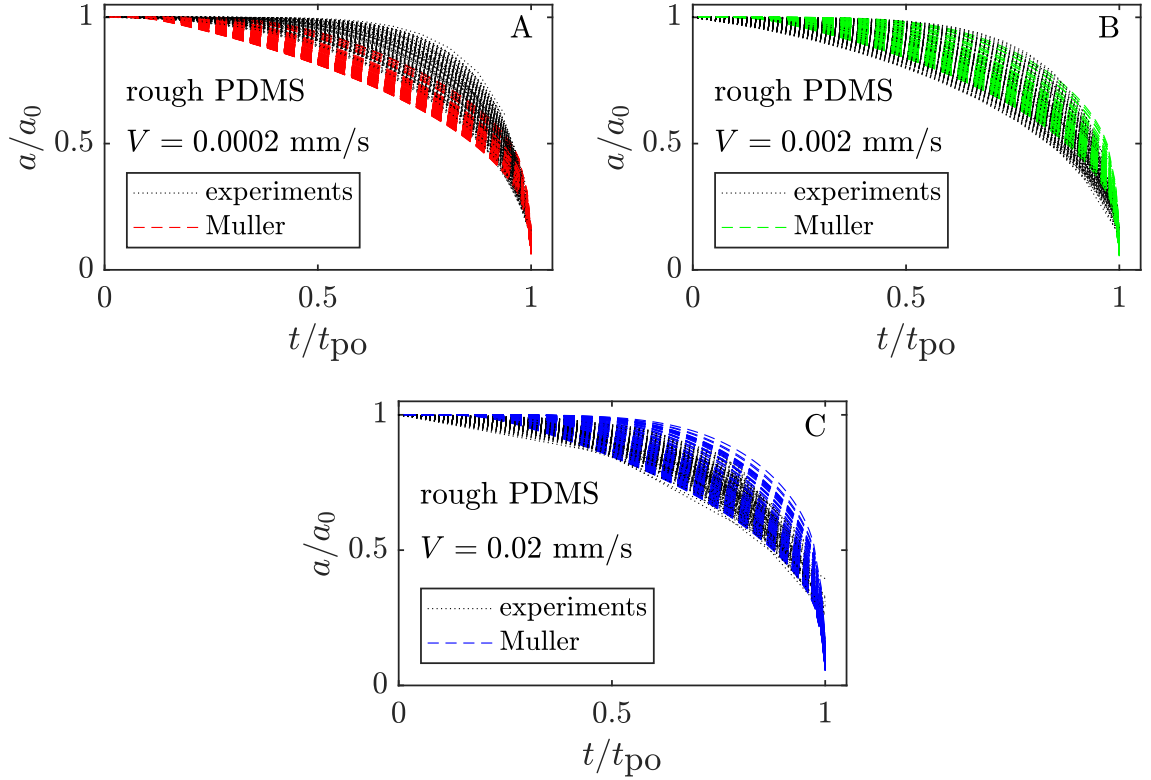


FIG. 9: A-C: The time dependence of the normalized contact radius  $a(t)$  for micro-contacts. Results are shown for unloading velocity of the indenter  $V = 0.0002, 0.002, 0.02$  mm/s (figs. A,B,C respectively). Black dotted lines denote experimental data, while colored dashed lines the Muller's model predictions.

For this reason, when increasing  $a_0$ , the  $a - t$  curve does not scale homothetically and a master curve cannot be found. This explains the scatter in fig. 9. However, an increasing trend of the pull-off time with  $a_0$  can be observed in our experimental data, as shown in figs. 10A-C, where results are presented for different unloading velocities. Anyway, as data are strongly scattered, a clear law of this increasing trend is not identified.

## Conclusions

In this paper, we have investigated the pull-off behavior of a rough contact interface between a smooth glass lens and a nominally flat viscoelastic substrate patterned with a height distribution of spherical micro-asperities. In the absence of any elastic coupling between micro-contacts, this system allows to measure simultaneously the pull-off behavior of a collection of micro-asperities contacts differing in their initial (equilibrium) adhesive

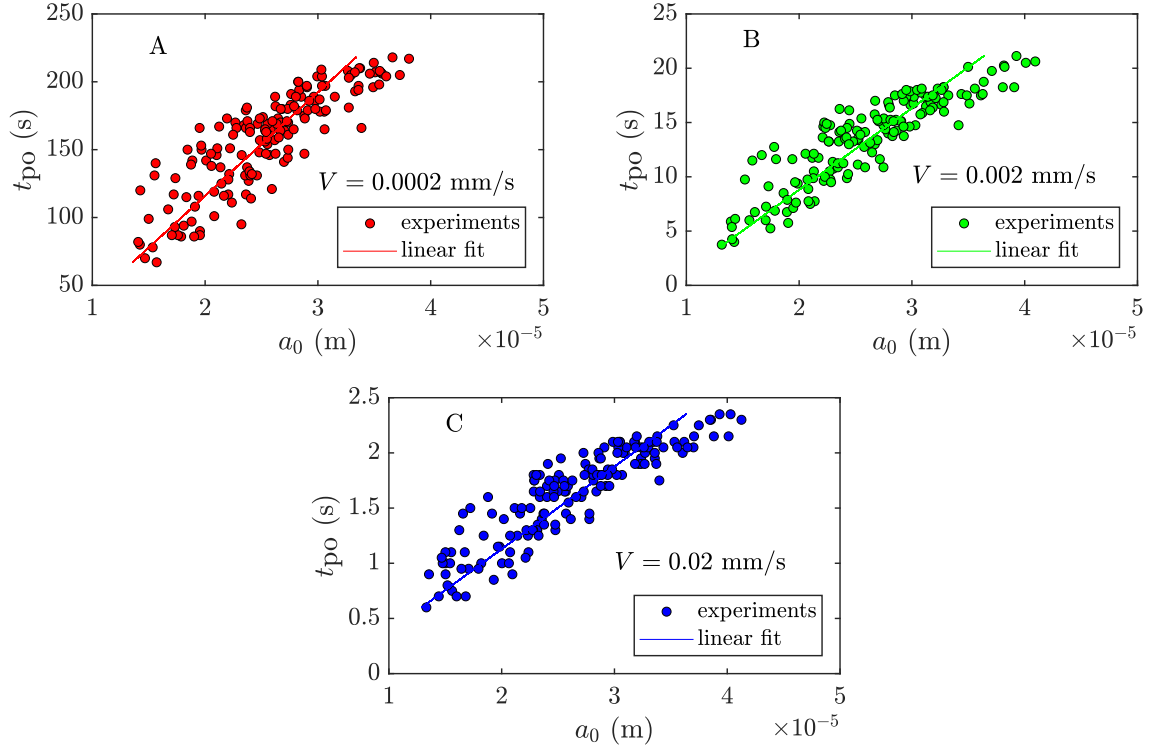


FIG. 10: A-C: The pull-off time  $t_{po}$  as a function of the initial contact radius  $a_0$ . Results are shown for rough PDMS and unloading velocity of the indenter  $V = 0.0002, 0.002, 0.02$  mm/s (figs. A,B,C respectively). Markers denote experimental data, while colored lines the corresponding linear fit; the  $R^2$  value is 0.73, 0.77 and 0.78 (figs. A,B,C respectively).

contact radius. From a comparison with macroscale pull-off experiments, it also offers the possibility to investigate the occurrence of scale effects in dissipative processes involved in adhesion.

Results show that the contact radius almost scales according to the ratio  $s_a = a_{0\text{macro}}/a_{0\text{micro}}$ , being  $a_0$  the initial radius measured at the beginning of the unloading process. Similarly, the contact line velocity  $v_c$  is found scaling with a factor  $s_v$  depending on the ratio  $s_a/s_t$ , where  $s_t = t_{po\text{-macro}}/t_{po\text{-micro}}$  and  $t_{po}$  is the time required for the pull-off to take place. Such results suggest that the nature of the dissipative processes involved in the pull-off of the adhesive contacts is almost scale independent from the millimeter size down to a few tens of micrometers. In other words, the assumption that viscoelastic losses are localized near the contact line in a region small with respect to the contact size remains valid at the micro-scale. Moving from this consideration, a simple theoretical procedure can be derived to evaluate the evolution of the contact radius  $a$  of micro-asperities contacts during unloading.

- 
- [1] Vakis, A. I., Yastrebov, V. A., Scheibert, J., Nicola, L., Dini, D., Minfray, C., ... & Molinari, J. F. (2018). Modeling and simulation in tribology across scales: An overview. *Tribology International*, 125, 169-199.
- [2] Kendall, K. (2007). *Molecular adhesion and its applications: the sticky universe*. Springer Science & Business Media.
- [3] Tiwari, A., Dorogin, L., Bennett, A. I., Schulze, K. D., Sawyer, W. G., Tahir, M., ... & Persson, B. N. J. (2017). The effect of surface roughness and viscoelasticity on rubber adhesion. *Soft Matter*, 13(19), 3602-3621.
- [4] Deplace, F., Carelli, C., Mariot, S., Retsos, H., Chateauminois, A., Ouzineb, K., & Creton, C. (2009). Fine tuning the adhesive properties of a soft nanostructured adhesive with rheological measurements. *The Journal of Adhesion*, 85(1), 18-54.
- [5] Majidi, C. (2014). Soft robotics: a perspective—current trends and prospects for the future. *Soft Robotics*, 1(1), 5-11.
- [6] Gebeshuber, I. C. (2007). Biotribology inspires new technologies. *Nano today*, 2(5), 30-37.
- [7] Lorenz, B., Krick, B. A., Mulakaluri, N., Smolyakova, M., Dieluweit, S., Sawyer, W. G., & Persson, B. N. J. (2013). Adhesion: role of bulk viscoelasticity and surface roughness. *Journal of Physics: Condensed Matter*, 25(22), 225004.
- [8] Johnson, K. L., Kendall, K., & Roberts, A. D. (1971). Surface energy and the contact of elastic solids. *Proceedings of the royal society of London. A. mathematical and physical sciences*, 324(1558), 301-313.
- [9] Greenwood, J. A., & Johnson, K. L. (1981). The mechanics of adhesion of viscoelastic solids. *Philosophical Magazine A*, 43(3), 697-711.
- [10] Gent, A. N., & Schultz, J. (1972). Effect of wetting liquids on the strength of adhesion of viscoelastic material. *The Journal of Adhesion*, 3(4), 281-294.
- [11] Maugis, D., & Barquins, M. (1978). Fracture mechanics and the adherence of viscoelastic bodies. *Journal of Applied Physics D: Appl. Phys.* 11 1989–2023
- [12] Robbe-Valloire, F., & Barquins, M. (1998). Adhesive contact and kinetics of adherence between a rigid cylinder and an elastomeric solid. *International Journal of adhesion and adhesives*, 18(1), 29-34.

- [13] Muller, V. M. (1999). On the theory of pull-off of a viscoelastic sphere from a flat surface. *Journal of Adhesion Science and Technology*, 13(9), 999-1016.
- [14] Barthel, E., & Haiat, G. (2002). Approximate model for the adhesive contact of viscoelastic spheres. *Langmuir*, 18(24), 9362-9370.
- [15] Haiat, G., Huy, M. P., & Barthel, E. (2003). The adhesive contact of viscoelastic spheres. *Journal of the Mechanics and Physics of Solids*, 51(1), 69-99.
- [16] Barthel, E., & Frétiigny, C. (2009). Adhesive contact of elastomers: effective adhesion energy and creep function. *Journal of Physics D: Applied Physics*, 42(19), 195302.
- [17] Yashima, S., Romero, V., Wandersman, E., Frétiigny, C., Chaudhury, M. K., Chateauinois, A., & Prevost, A. M. (2015). Normal contact and friction of rubber with model randomly rough surfaces. *Soft Matter*, 11(5), 871-881.
- [18] Acito, V., Ciavarella, M., Prevost, A. M., & Chateauinois, A. (2019). Adhesive contact of model randomly rough rubber surfaces. *Tribology Letters*, 67(2), 54.
- [19] Roberts, A. D. (1979). Looking at rubber adhesion. *Rubber Chemistry and Technology*, 52(1), 23-42.
- [20] Violano, G., & Afferrante, L. (2019). Adhesion of compliant spheres: an experimental investigation. *Procedia Structural Integrity*
- [21] Andrews, E. H., & Kinloch, A. J. (1973). Mechanics of adhesive failure. II. Proceedings of the Royal Society of London. A. Mathematical and Physical Sciences, 332(1590), 401-414.
- [22] Gent, A. N., & Petrich, R. P. (1969). Adhesion of viscoelastic materials to rigid substrates. Proceedings of the Royal Society of London. A. Mathematical and Physical Sciences, 310(1502), 433-448.
- [23] Kendall, K. (1973). Shrinkage and peel strength of adhesive joints. *Journal of Physics D: Applied Physics*, 6(15), 1782.
- [24] Williams, Malcolm L., Landel, Robert F., Ferry, John D. (1955). "The Temperature Dependence of Relaxation Mechanisms in Amorphous Polymers and Other Glass-forming Liquids". *J. Am. Chem. Soc.* 77 (14): 3701-3707.
- [25] Ramond, G., M. Pastor, D. Maugis, and M. Barquins. "Mesure du module complexe par poinçonnement." *Cahiers du Groupe Français de Rhéologie* 6, no. 67 (1985): 3-3.
- [26] Charmet, J. C., Vallet, D., & Barquins, M. (1998). Surface and bulk properties in Adherence of Elastic-Viscoelastic Solids.

- [27] Palchesko, R. N., Zhang, L., Sun, Y., & Feinberg, A. W. (2012). Development of polydimethylsiloxane substrates with tunable elastic modulus to study cell mechanobiology in muscle and nerve. *PloS one*, 7(12).
- [28] Violano, G., & Afferrante, L. (2019). Modeling the adhesive contact of rough soft media with an advanced asperity model. *Tribology Letters*, 67(4), 119.
- [29] Violano, G., & Afferrante, L. (2019). On DMT methods to calculate adhesion in rough contacts. *Tribology International*, 130, 36-42.
- [30] Afferrante, L., Bottiglione, F., Putignano, C., Persson, B. N. J., Carbone, G. (2018). Elastic Contact Mechanics of Randomly Rough Surfaces: An Assessment of Advanced Asperity Models and Persson's Theory. *Tribology Letters*, 66, 75.
- [31] Barquins, M. (1983). Influence of the stiffness of testing machines on the adherence of elastomers. *Journal of applied polymer science*, 28(8), 2647-2657.
- [32] Baek, D., Hemthavy, P., Saito, S., & Takahashi, K. (2017). Evaluation of energy dissipation involving adhesion hysteresis in spherical contact between a glass lens and a PDMS block. *Applied Adhesion Science*, 5(1),1-11.